

# Residual stress measurements of conventional and stress peen formed 2024–T3 aluminum sheets

Pierre A. Fauchaux, Hong Yan Miao, Martin Levesque, Frédéric P. Gosselin

*Laboratory for multiscale mechanics (LM2), Département de Génie Mécanique, Ecole Polytechnique de Montréal, Montréal, QC, Canada*

---

## Abstract

Aluminum skins on the lower wings of most commercial aircraft are shaped using shot peen forming. This process, which involves bombarding the skins with hard shot, uses nonuniform plastic flow to induce curvatures—in the same way that differential expansion makes metal bilayers bend when heated. Here, we investigate experimentally how constraining conditions affect the final shape of peen formed parts. We report peen forming experiments for 4.9 mm thick rectangular 2024–T3 aluminum sheets of different aspect ratios uniformly shot peened on one face with a low intensity saturation treatment. Some specimens were free to deform during peening while others were elastically prestressed in a four-point bending jig. For each aspect ratio and prestress condition, residual stresses were measured near the peened surface

---

\*Corresponding author

*Email address:* frederick.gosselin@polymtl.ca (Frédéric P. Gosselin)

*URL:* <http://www.polymtl.ca/lm2> (Frédéric P. Gosselin)

with the hole drilling method. Additional residual stress profiles were also obtained with the slitting method. The residual stress measurements show that the progressive deformation of unconstrained specimens had the same effect as an externally applied prestress. For the peening conditions investigated, this progressive deformation caused unconstrained strips to exhibit curvatures 33 % larger than identical strips held flat during peening. Furthermore, we found that the relative importance of material anisotropy and geometric effects did determine the bending direction of unconstrained specimens.

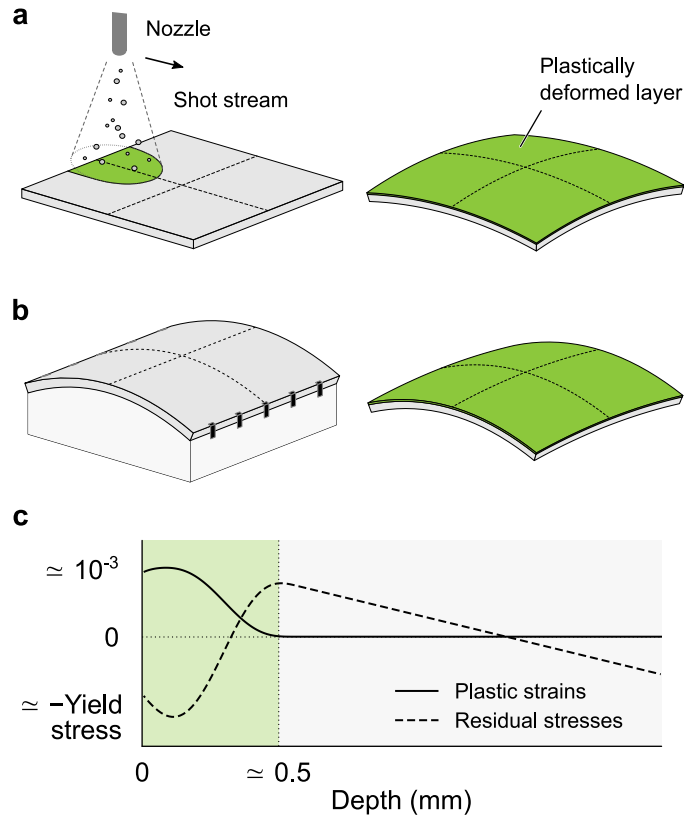
*Keywords:* Initial stress, peen forming, plastic strain, residual stress, 2024-T3 aluminum alloy

---

## 1. Introduction

Shot peen forming stands out among sheet metal forming processes by its flexibility and low operating costs. The process consists in bombarding thin metal parts with hard shot such that the incompatibility of deformations  
5 between the plastically deformed surface layers and the underlying material causes the part to bend, as illustrated schematically in Figure 1a. Typical applications include forming large wing-skin panels for commercial aircraft [1, 2], forming doubly curved panels for space launchers [3, 4], and correcting small out-of-tolerance distortions on machined parts [5, 6].

10 Because peening stretches the material in all directions, uniformly peened parts tend to deform into spherical shapes, as illustrated in Figure 1a. To break this symmetry, process engineers use a technique called stress peen



**Figure 1.** Peen forming of a metal plate. Repeated impacts plastically deform a thin layer of material which, as it stretches, causes the plate to deform. (a) Plates peened with low intensity treatments, thick plates, and plates with high aspect ratios tend to deform into spherical shapes. (b) Prebending a plate during peening results in larger curvatures in the prestress direction and smaller curvatures in the transverse direction. (c) Typical in-plane plastic strain and residual stress profiles after uniform peening. The in-plane expansion of the upper layers is resisted by the bulk, which causes compressive residual stresses near the surface. Conversely, the upper layers stretch the bulk, which causes tensile stresses deeper into the material. In the bulk, stresses vary linearly owing to the stretching and bending of the specimen.

forming where jigs are used to hold parts into a bent shape during peening. This results in larger curvatures in the bending direction and smaller  
15 curvatures in the transverse direction, as illustrated in Figure 1b. The final curvatures of stress peen formed parts was repeatedly observed to be proportional to the prestress curvature. Table 1 compiles the publicly available results we found on stress peen forming of uniformly peened rectangular plates.

20 While many experimental studies dedicated to shot peening investigated residual stresses, roughness, and changes in microstructure induced by peening treatments, see for example the the literature reviews of [7], comparatively fewer considered peening induced distortions. Among these, most aimed at generating data to establish process parameters for a given application. For  
25 example, [8] investigated the influence of shot size, shot velocity, and the plate's aspect ratio on the curvature of 610 mm long 2024 and 7050 rectangular aluminum sheets that were free to deform during peening; [9] generated a dataset of curvature and residual stress profiles for  $400 \times 50$  mm 7050 and 7475 aluminum strips for various prestress conditions; and [10] reported similar  
30 results for  $76 \times 19$  and  $76 \times 76$  mm 2024–T3 aluminum strips. Additional references featuring conventional and stress peen forming experimental results are listed in Tables 1 and 2.

Of these studies, only half report curvature measurements in more than one direction, and only three report residual stress measurements in more than



35 one direction. However, several phenomena are expected to cause anisotropic curvatures and residual stresses. These include the known plastic anisotropy of rolled aluminum sheets used for most experiments [11], anisotropic initial residual stresses inherited from the manufacturing process of the sheets (e.g., quenching or rolling), and prestress, whether externally applied with  
40 a jig (Figure. 1b) or resulting from the progressive deformation of an unconstrained part (Figure. 1a). Although these phenomena were suspected to account for most of the discrepancies between experiments and numerical simulations of the process previously reported by our team in [12] and [13], this intuition could not be confirmed at the time due to a lack of experimental  
45 data.

In this paper, we investigate experimentally the effect of material anisotropy and prestress on the final deformed shape of uniformly peened aluminum sheets. The paper is structured as follows. Section 2 presents the materials and methods. Section 3 summarizes the results of (i) conventional peen  
50 forming experiments conducted on 4.9 mm thick and 1016 mm long 2024-T3 aluminum alloy rectangular sheets of different aspect ratios and (ii) stress peen forming experiments conducted on  $508 \times 127$  mm strips of the same alloy. These tests probed the influence of the alignment of the specimens with respect to the rolling direction, that of their aspect ratio, and, to a lesser  
55 extent, that of the peening trajectory on curvatures and residual stresses. Finally, Section 4 presents a preliminary, qualitative, analysis of the results.

**Table 1**

Compilation of publicly available papers and reports featuring stress peen forming experimental results for uniformly peened rectangular plates. Not included are several conference papers that were not readily available, and papers written in languages that none of the authors were familiar with. This includes some possibly highly relevant studies in the German, Chinese, and Japanese-speaking literature. Brackets indicate ranges.

Reference	Material	Dimensions			Peening treatment <sup>a</sup>				Increment in curvature per unit increment in prestress curvature		Reported results		Notes
		Length (mm)	Width (mm)	Thickness (mm)	Media <sup>b</sup>	Coverage <sup>c</sup> (%)	Intensity <sup>d</sup> ( $\times 10^{-3}$ in)	Prestress radius of curvature (mm)	Along prestress direction (-)	Along transverse direction (-)	Deformed shape	Residual stress <sup>e</sup>	
[14]	7075-T7651 Al.	762	508	17.3	Saturation: 0.6 mm steel Forming: 3.2 mm steel	Saturation: 100 Forming: between 60 and 80	Saturation: $\approx 6$ A Forming: -	1700 (along short side)	-	-	-	Profiles, some in both directions (XRD)	†
[15]	2024-T351 Al.	67	67	4	Laser peening	-	-	$\infty$ , 2000, 1000, 667	0.44	0.14	Curvature along both directions; Some 3D scans	Surface stress (XRD)	†
[16]	LY12CZ Al.	76	76	2	[2, 2.5] mm iron	100	-	$\infty$ , 5000, 1000, 500, 250	0.60 <sup>f</sup>	-0.06 <sup>f</sup>	Arc height	-	†
[10]	2024-T3 Al.	76	19	1.6	Z425	100	5, 7.4, 8.7 A	$\infty$ , 720, 360, 240	[0.41, 0.65]	-	Arc height (in both directions for square specimens); some line scans	Profiles along prestress direction (XRD)	†, ‡
[17]	2024-T3 Al.	76	76	1.6	Z425	100	5, 7.4, 8.7 A	$\infty$ , 720, 360, 240	[0.40, 0.65]	[-0.08, -0.17]	Arc height (in both directions for square specimens); some line scans	Profiles along prestress direction (layer removal)	-
[5]	7075-T7651 Al.	305	44	6.35	Saturation: S230 Forming: 3/16" ball bearings	Saturation: 100 Forming: 20, 40, 60, 80	Saturation: 6 A Forming: 10, 12, 15 C	$\infty$ , 1950, 825, 625	-	-	-	Profiles along prestress direction (layer removal)	-
[9]	7050-T7451 Al.	400	50	2, 5, 10, 15	S230, S550, 1/8"	From 60 to 200	-	1270, 850, 420, 170 <sup>g</sup>	-	-	Curvature along prestress direction	Profiles along prestress direction (XRD)	†
[18]	7150 Al.	300	200	8, 10, 12	3.18 mm	From $\approx 50$ to 100	-	810, 680, 540	-	-	Curvature along prestress direction	-	-
[19]	2024-T351 Al.	100	30	5	Brinell indenter (3.175 mm diam.) 3.175 mm steel	Variable	-	$\infty$ , 1252, 626	[0.27, 0.46] <sup>h</sup>	[-0.21, -0.12] <sup>h</sup>	Curvature along both directions	-	†
[20]	2024-T351 Al.	120	50	1.5, 2.0, 2.5, 3.0, 3.5	Ultrasonic peening (indenter 3 mm in diam.)	-	-	$\infty$ , 1200, 1000, 800, 600, 400	0.63 <sup>i</sup> 0.48 <sup>i</sup> 0.38 <sup>i</sup> 0.33 <sup>i</sup> 0.33 <sup>i</sup>	-0.05 <sup>i</sup> -0.05 <sup>i</sup> -0.05 <sup>i</sup> -0.08 <sup>i</sup> -0.07 <sup>i</sup>	Curvature along both directions	-	-
This study	2024-T3 Al.	508	127	4.9	SCCW28	100	12 A	$\infty$ , 3704, 1961, 1205, 952	[0.22, 0.23]	[-0.03, -0.13]	Curvature along both directions	Profiles in both directions (hole drilling)	†, ‡

<sup>a</sup> Process parameters such as air pressure, mass flow, and exposure time are usually available when intensity or coverage are not reported.  
<sup>b</sup> Conventional designation or diameter.  
<sup>c</sup> As defined in [21], unless otherwise specified.  
<sup>d</sup> Almen intensity, as defined in [22], unless otherwise specified.  
<sup>e</sup> XRD stands for X-ray diffraction.  
<sup>f</sup> Estimated from table 1 of [16]. The curves deviate from linearity for prestress radii of curvature larger than 4000 mm.  
<sup>g</sup> Computed from beam bending theory as  $hE/2\sigma$ , where  $h$  is the thickness of the plate,  $E$  is Young's modulus, and  $\sigma$  is 90% of the yield stress.  
<sup>h</sup> Estimated from figure 21 of [19].  
<sup>i</sup> Estimated from figure 11 of [20].  
<sup>j</sup> Large dispersion in results.  
<sup>k</sup> Results on unconstrained strips also available.  
<sup>l</sup> Features finite element impacts simulations.  
<sup>m</sup> Half the specimens was cut with the long side aligned with the rolling direction while the other half was cut with the long side aligned with the transverse direction.

**Table 2**

Compilation of publicly available papers and reports featuring shot peened forming experimental results for uniformly peened rectangular plates. Not included are several conference papers that were not readily available, and papers written in languages that none of the authors were familiar with. This includes some possibly highly relevant studies in the German, Chinese, and Japanese-speaking literature.

Reference	Material	Dimensions			Peening treatment <sup>a</sup>					Reported results	
		Length (mm)	Width (mm)	Thickness (mm)	Media <sup>b</sup>	Coverage <sup>c</sup> (%)	Intensity <sup>d</sup> ( $\times 10^{-3}$ in)	Shot speed (m/s)	Specimens constrained during peening	Deformed shape	Residual stress <sup>e</sup>
[23]	SAE 1070 steel	75	19	1.29	Similar to S110	Variable	8 A	45	Yes	Curvature in both directions; one line scan	Profiles in both directions (XRD)
[24]	2024-T62 Al. 7075-T76 Al.	360	130	4.5 4.0	From S230 to S280	100	7 A, 5 C	-	No	Deflection; one line scan	-
[13]	2024-T3(51) Al.	1000	1000	5, 10, 15	S230 1/8" steel	100	16.8 A 22.9 C	-	No	Curvature in both directions; some line scans	Profiles on thick blocks in one direction (XRD)
		200	50	10	S230 1/8" steel	100	16.8 A 22.9 C				
[12]	2024-T3 Al.	76	19	1.6	Z425	Variable	-	34, 52	Yes	Arc height; curvature in both directions	Initial stress profiles in both directions (XRD)
[25] <sup>f</sup>	Inconel 718	75	19	5.0, 2.0	S130	125 200	5.1 A 9.1 A	$\approx 42$	Yes	3D scans, some line scans	Profiles in both directions (XRD)
[26]	HE 30 Al., mild steel, pure copper	76	25	3.2	S170, S240	Variable	-	-	Yes	Arc height	-
[8]	2024-T3(51) and 7050-T6(51) Al.	610	152, 305, 610 <sup>g</sup>	1.6, 4.6, 12.7	0.6 mm steel 1.0 and 1.7 mm steel	Variable	8, 10, 16 A -	32, 53, 78	No	Curvature in both directions	Typical values (XRD)
[10], [27]	2024-T3 Al.	76	19, 76	1.6	Z425	Variable	5 A 7.4 A 8.7 A	35 54 66	Yes	Arc height; curvature in both directions for square specimens	Through thickness profiles on specimens and thick blocks along one direction (XRD)
[9]	7050-T7451 and 7475-T7451 Al.	400	50	2	S230	Variable	-	50, 61, 72	Some specimens	Curvature along long side	Profiles along one direction for some 7050 Al. specimens (XRD)
				5	S230			50, 61, 72			
				5	S550			16, 22, 29			
				10	S550			16, 22, 29			
				10	1/8" steel			13, 17, 19			
15	1/8" steel	13, 17, 19									
Present study	2024-T3 Al.	1016	254, 508, 1016	4.9	SCCW28	100	12 A	41	No	3D scans	Profiles in both directions (hole drilling, slitting)

<sup>a</sup> Process parameters such as air pressure, mass flow, and exposure time are usually available when intensity or coverage are not available.

<sup>b</sup> Conventional designation or diameter.

<sup>c</sup> As defined in [21], unless otherwise specified.

<sup>d</sup> Almen intensity, as defined in [22], unless otherwise specified.

<sup>e</sup> XRD stands for X-ray diffraction.

<sup>f</sup> Also reported are microstructural characterization (including EBSD maps), some initial stress profiles, FWHM of XRD measurements, microhardness measurements, and experiments on specimens of complex geometries.

<sup>g</sup> Limited results for specimens of other aspect ratio are available in figure 11 of [8].

**Table 3**

Mean static properties of the 4.9 mm thick aluminum alloy 2024–T3 sheets tested in this work. These values were averaged over three tests.

Angle w.r. to rolling direction (°)	Young’s modulus (GPa)	Yield stress at 0.2 % (MPa)	Ultimate tensile stress (MPa)	Elongation at fracture (mm/mm)
0	$71.5 \pm 1.6$	$381 \pm 0$	$486 \pm 1$	$0.1836 \pm 0.0070$
45	$71.6 \pm 3.0$	$349 \pm 1$	$485 \pm 0$	$0.1920 \pm 0.0145$
90	$71.7 \pm 1.5$	$339 \pm 1$	$489 \pm 0$	$0.1946 \pm 0.0058$

Mean  $\pm$  95 % confidence interval

## 2. Materials and methods

*Material.* All experiments were conducted on 4.9 mm thick Kaiser Stretched aluminum alloy 2024–T3 sheets purchased from Kaiser Aluminum. The manufacturing process of the sheets included a stress relief by a stretching step. Metallographic specimens etched with Keller’s reagent revealed large elongated grains of mean aspect ratio 7.1:3.6:1.0 along the longitudinal (L), long transverse (T), and short transverse (S) directions, respectively. Grains had an average length of 0.268 mm. The largest observed grain length was of 4.7 mm. Static properties were obtained from tensile tests performed at 0°, 45°, and 90° from the rolling direction, as per [28]. Three specimens in each direction were removed from the same sheet (the consistency of properties from one sheet to the next was not assessed). Table 3 lists the measured static properties for each direction. The observed elastic isotropy and mild plastic anisotropy are consistent with other experimental data from the literature [29, 30].

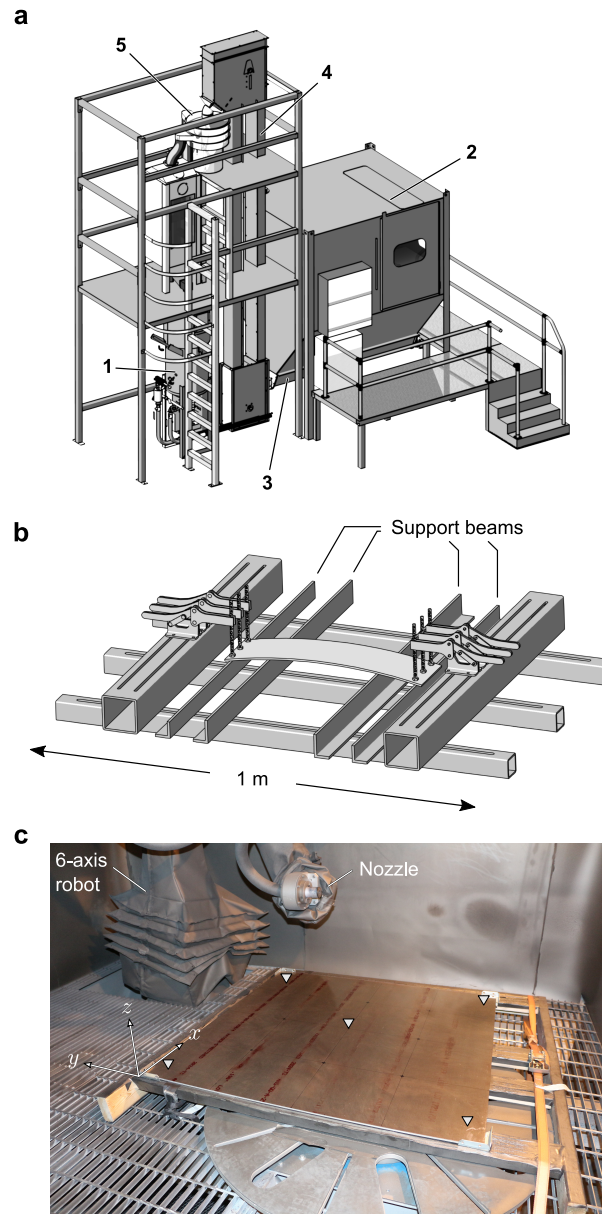
*Peening setup.* All specimens were shot peened in the Canablast compressed-air cabinet shown in Figure 2a. The peening cell was equipped with a 6-axis robotic arm for an accurate positioning of the nozzle (M-20iA supplied by Fanuc), with a particle velocity sensor to measure the average shot velocity (Shotmeter G3 supplied by Progressive Technologies), and with a GoPro digital camera to record the peening process application. Shot were recycled. Torn and broken shot were removed by separator screens.

For conventional peen forming experiments, the frame shown in Figure 2c provided a level working surface and stops guaranteed consistent positioning from one specimen to the next. The specimens were otherwise free to deform during peening.

For stress peen forming experiments, specimens were prestressed in the four-point bending jig shown in Figure 2b. The spacing between the 4 support beams could be adjusted and several pairs of beams of different heights were used to obtain prestress curvatures ranging from 0 to  $10.5 \times 10^{-4} \text{ mm}^{-1}$  (or, equivalently, radii of curvatures ranging from infinity to 952 mm).

*Peening treatment.* High hardness spherically conditioned cut wire steel shot SCCW28 compliant with [31] were used for all treatments. The manufacturer's specification stated a 55–62 HRC hardness and a nominal diameter of 0.71 mm.

The same treatment, representative of low intensity saturation treatments used in the industry, was applied to all specimens. The nominal peening



**Figure 2.** Shot peening setup. (a) Compressed air peening cabinet used for peen forming experiments. Shot are propelled from a pressurized tank (1) into a closed cabinet (2) where they strike the parts. Used shot are collected at the bottom of the cabinet by an endless screw (3) followed by an elevator bucket (4). They are dropped onto a stack of separator screens (5) that removes broken shot before recycling them into the tank. (b) Four-point bending jig used for stress peen forming experiments. The spacing between the 4 support beams could be adjusted. Several pairs of beams of different heights were used to obtain curvatures ranging from 0 to  $10.5 \times 10^{-4} \text{ mm}^{-1}$  (associated radii of curvature: from infinity to 952 mm). (c) Interior of the peening cabinet showing the robotic arm and an unpeened  $1016 \times 1016 \text{ mm}$  sheet resting on a leveled frame. During conventional peen forming experiments, the sheets were free to deform. Downward pointing triangles show the locations at which Almen intensity was measured.

**Table 4**

Peening parameters used to obtain a  $12 \times 10^{-3}$  inches A Almen intensity and 100 % coverage with SCCW28 shot.

Nozzle diameter (mm)	Air pressure (Bars)	Mass flow (kg/s)	Shot speed <sup>†</sup> (m/s)	Stand-off distance (cm)	Offset between strokes (mm)	Peening speed (cm/s)	Number of cycles
12.7	1.72	0.12	41	41	67	15	12

<sup>†</sup> Average speed at the exit of the nozzle.

parameters were a 12A (0.30 mmA) Almen intensity and 100 % coverage,<sup>1</sup>  
 95 which were obtained with the process parameters listed in Table 4. All peening experiments were conducted as per [21, 22, 32]. Almen tests ran at the five locations indicated by downward pointing triangles in Figure 2c yielded intensities ranging from 11.6 A(0.26 mmA) to 12.0 A(0.30 mmA), which substantiates that intensity was uniform over the working surface. Consistency of the process was ensured by performing additional Almen tests at  
 100 the center of the specimens at the beginning and at the end of each peening day, or after having peened two plates, whichever was the shortest.

*Distribution of impacts after one peening stroke.* The distribution of impacts after one peening stroke was characterized by peening a  $508 \times 203$  mm dummy

---

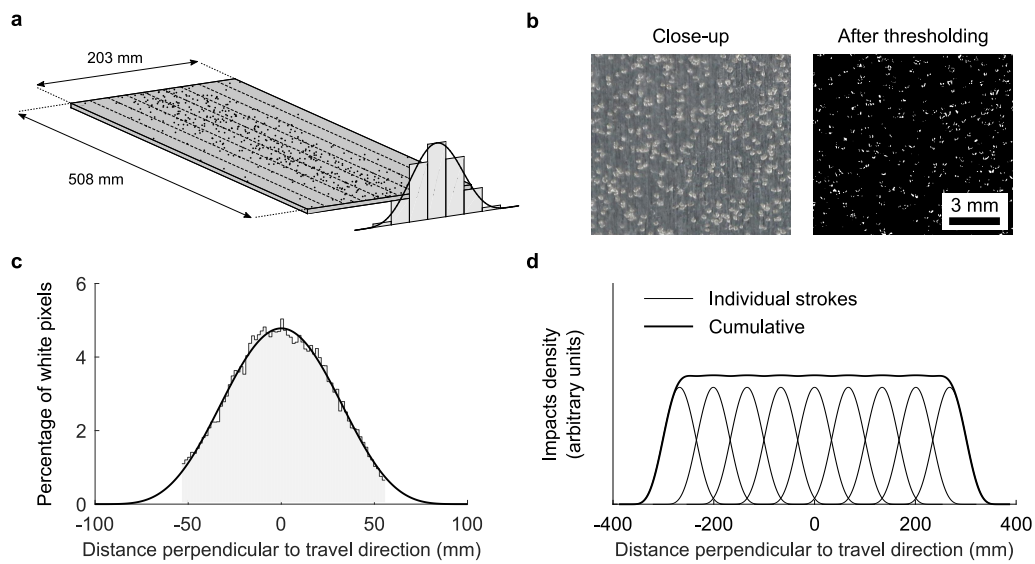
<sup>1</sup>Alongside shot specifications, Almen intensity and coverage are the two parameters used to characterize peening treatments in the industry. Coverage is the fraction of a surface covered by dents. Intensity is primarily intended as a process control parameter. It is obtained by (i) peening normalized SAE-1070 spring steel strips mounted on a holding fixture in the same conditions as production parts for increasing amounts of time, (ii) measuring their deflection in a standardized Almen gage, and (iii) plotting the deflection as a function of peening time. From these curves, intensity is defined as the value of the deflection which increases by 10 % when the peening time is doubled [22].

specimen, the same 2024–T3 aluminum as the test specimens, with the nozzle moving at 22.5 cm/s. At that speed, the density of impacts was low and there was little overlap between dimples. High resolution pictures of the peened surface were taken as the specimen was lit with softened raking lights. The pictures were then stitched together, binarized, and partitioned into bins parallel to the peening direction as shown in Figure 3a–b. The distribution of impacts was subsequently estimated by counting the fraction of white pixels in each bin. Note that, although the shape of white spots on binarized images was markedly different from that of the dimples, their location was correct and it was assumed that variations in shape from one spot to the next were compensated by the many impacts considered. Figure 3c shows the distribution of white pixels as well as a least-squares fit of the data with equation

$$f(x) = A \left( 1 - 4 \left( \frac{x}{w} \right)^2 \right)^{\beta-1},$$

where  $A = 4.78$  is the amplitude in % of white pixels,  $w = 205$  mm is the width, and  $\beta = 6.32$  is a dimensionless adjustable parameter. Superimposing  
105 several of these distributions allows to estimate the uniformity of the number of impacts per unit surface after several parallel overlapping strokes, as shown in Figure 3d. In this case, we found that the largest spacing between parallel strokes that yielded variations smaller than 1% in the number of impacts per unit surface was 67 mm.





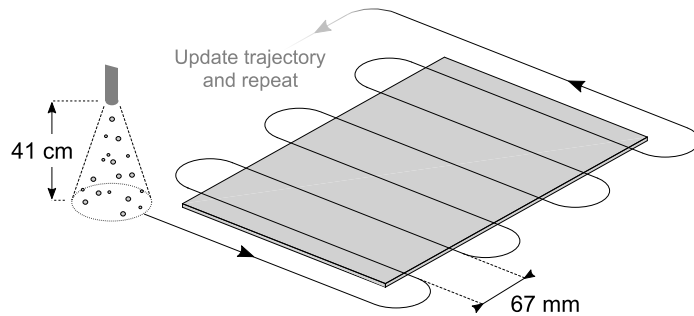
**Figure 3.** The density of impacts after a single straight peening stroke was characterized by (a) peening a dummy specimen, (b) thresholding high resolution pictures of the peened surface such that dimples appeared as white spots, and (c) counting the fraction of white pixels in bins parallel to the peening stroke. (d) The density of impacts after several parallel overlapping strokes was estimated by superimposing several of these distributions. In (d), the distributions for individual strokes are spaced 67 mm apart.

*Peening trajectories.* All specimens were peened with a succession of parallel strokes, as shown in Figure 4. To ensure that the nozzle remained approximately normal to the peened surface as specimens deformed, the treatment was broken into 12 cycles and the trajectory for cycle  $n + 1$  was computed based on the shape of the specimen at the end of cycle  $n$ . The latter was estimated by recording the position of target points drawn on the peened surface with a stylus mounted on the head of the 6-axis robot and by fitting a surface of equation

$$z(x, y) = ax^2 + by^2,$$

110 through these points, where  $a$  and  $b$  are adjustable parameters and  $x$ ,  $y$ , and  $z$  are defined in the plane of the flat plate as shown in Figure 2c. To achieve uniform coverage, the offset between two successive strokes was set to 67 mm based on the analysis of the distribution of impacts from the previous paragraph. Visual inspection confirmed that coverage was uniform. The  
 115 peening speed listed in Table 4 was set so that 100% coverage was reached after 12 peening cycles. Coverage was estimated as per [21] from magnified pictures of the peened surface.

*Specimens.* For comparison purposes, specimens similar to those used in Kulkarni et al. [8] were selected for conventional peen forming experiments.  
 120 The specimens consisted of 10 rectangular sheets of 4:1, 2:1, 1:1, 1:2, and 1:4 aspect ratio, 1016 mm along the long side. Two sheets were peened per aspect ratio. Half of the specimens were peened with strokes parallel to the



**Figure 4.** Nozzle trajectory for the first peening cycle. The trajectory was updated at the end of each cycle based on the current shape of the part so that the nozzle remained normal to, and at a constant distance from, the surface. Half of the specimens was peened with strokes parallel to the L direction while the other half was peened with strokes parallel to the T direction.

L direction while the other half were peened with strokes parallel to the T direction. Table 5 lists the specimens used for conventional peen forming experiments.

Specimens used for stress peen forming experiments were  $508 \times 127$  mm strips. The prestress curvatures were 0, 2.7, 5.1, 8.3, and  $10.5 \times 10^{-4} \text{ mm}^{-1}$ . Strips with zero prestress curvature were held flat during peening. These curvatures induce stresses of 0, 47, 90, 146, and 184 MPa on the upper face of the strips, which is well below the yield stress of the material. Two strips with their long side aligned with the L direction and two strips with their long side aligned with the T direction were peened for each prestress condition, except for the  $8.3 \times 10^{-4} \text{ mm}^{-1}$  prestress condition where three strips were used. All strips were peened with strokes parallel to their long side.

**Table 5**

Specimens used for conventional peen forming experiments.

Specimen ID	Dimensions (mm)		Peening strokes	Residual stress measurements
	Along L	Along T		
Sheet 4:1-L	1016	254	Parallel to L	Hole drilling
Sheet 2:1-L	1016	508		-
Sheet 1:1-L	1016	1016		Hole drilling
Sheet 1:2-L	508	1016		Hole drilling, Slitting
Sheet 1:4-L	254	1016		Hole drilling, (XRD)
Sheet 4:1-T	1016	254	Parallel to T	(XRD)
Sheet 2:1-T	1016	508		Hole drilling
Sheet 1:1-T	1016	1016		(XRD)
Sheet 1:2-T	508	1016		-
Sheet 1:4-T	254	1016		-

135 *3D scans and curvature measurements.* After peening, all sheets used for  
conventional peen forming experiments were scanned with a coordinate mea-  
suring machine (Mitutoyo, Crysta-Apex 163011) equipped with a REVO®  
5-axis measurement system. Measurements were taken every 4 mm in con-  
tinuous scanning mode along several lines parallel to the long and the short  
140 directions.

Strips used for stress peen forming experiments were scanned along the lines  
parallel to the long and short directions passing through the center of the  
specimens (i) before peening while held in the prestressing jig and (ii) after  
peening after all constraints had been released. Measurements while on the  
145 prestressing jig were taken every 25 mm with a stylus mounted on the head  
of the 6-axis robot. Measurements after peening were taken every 3 mm with  
an electronic indicator (CDI Chicago, Logic ALG, A2720).

Coupons used for residual stress measurements (see next paragraph) were also scanned with an electronic indicator, as just described.

150 Curvatures were computed as  $\kappa = p''/(1 + p'^2)^{3/2}$ , where  $p$  is an eighth-order polynomial fit to the 3D scans along the dotted lines shown in Figure 1a and where the prime denotes differentiation with respect to the direction along which the curvature is computed. All curvatures reported in the rest of the article are average curvatures averaged over the central 50 % of the scanning  
155 lines.

*Residual stress measurements.* Due to its high sensitivity to low residual stress levels [33], the slitting method was used to characterize initial residual stresses on as-rolled sheets. Hill-Engineering performed the measurements on two  $51 \times 51$  mm coupons (one coupon for each direction). A single strain gage  
160 located opposite to the cut on the back face of the specimens was used. The slot was incrementally cut by wire electric discharge machining by 0.051 mm to 0.254 mm increments over the first 3.43 mm. Residual stresses were computed as described in Schajer and Prime [34], with unit pulse basis functions, Tikhonov regularization, and compliances computed from 2D plane-strain fi-  
165 nite element simulations. The procedure used for uncertainty analysis is detailed in Prime and Hill [35].

The incremental hole drilling method was used to measure residual stresses in

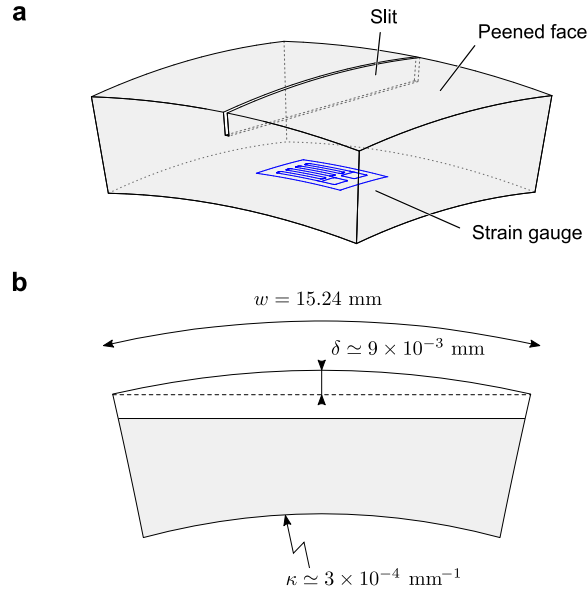
- $254 \times 254$  mm coupons removed from selected specimens used for con-

170       ventional peen forming experiments (one coupon per aspect ratio; see  
Table 5);

- $254 \times 127$  mm coupons removed from some strips used for stress peen forming experiments (one coupon per prestress condition).

The coupons were removed from the center of the sheets with a lubricated  
175 jigsaw (except for sheet 1:4-L for which the coupon was removed from the  
end). Residual stresses were measured at the center of the coupons, far away  
from the edges, to minimize the effect of cutting induced plastic deformations  
and heating on measurement. Hill-Engineering, performed all measurements  
as per [36]. The holes were 2 mm in diameter and were drilled in 0.051 mm  
180 increments to a final depth of 1.020 mm. Uncertainty calculations—which  
are not part of [36]—were similar to those used for slitting measurements.

One additional slitting measurement was performed on sheet 1:2-L to vali-  
date the hole drilling measurements. Two  $15.24 \times 17.78$  mm coupons were  
removed by electric discharge machining 2.5 cm away from the edges of the  
185 coupon used for hole drilling measurements. Such small coupons were needed  
to ensure that the depth of the slot was approximately constant as slot cut  
with straight EDM wires into curved specimens are deeper at the center  
than they are near the edges, as illustrated in Figure 5. The curvature of  
the coupons was estimated to  $3 \times 10^{-4} \text{ mm}^{-1}$ , which gave a variation in the  
190 depth of the cut of  $\delta \simeq \kappa w^2/8 \simeq 9 \times 10^{-3}$  mm when cutting along the short  
side, where  $\kappa$  and  $w$  are defined as in Figure 5b. Such variations were a



**Figure 5.** Schematic illustration of the specimens used to measure peening-induced residual stresses with the slitting method (curvature amplified for clarity). (a) Strains were measured with a single strain gauge attached to the back face of the specimens as the latter were cut with a straight EDM wire. (b) Since peened specimens are curved, the slot is deeper near the center than it is near the edges. Because slitting returns stresses averaged over the length of the slot, small  $15.24 \times 17.78 \text{ mm}$  coupons were used so that the variation in the depth of the slot, which was estimated to  $\delta \simeq 9 \times 10^{-3} \text{ mm}$  from the curvature of the coupons, was small, when compared to the characteristic length over which residual stresses varied (see Figures 9 and 10a).

posteriori confirmed to be much smaller than the characteristic length over which residual stresses varied (see Figures 9 and 10a).

X-ray diffraction measurements were attempted on several specimens (Table 5) but the large grain size and texture of the material prevented obtaining meaningful results.

*Additional information.* Additional details about experimental conditions, videos of the peening treatments, 3D scans of the specimens, and tabulated

residual stress profiles are provided as supplementary material.

## 200 **3. Results**

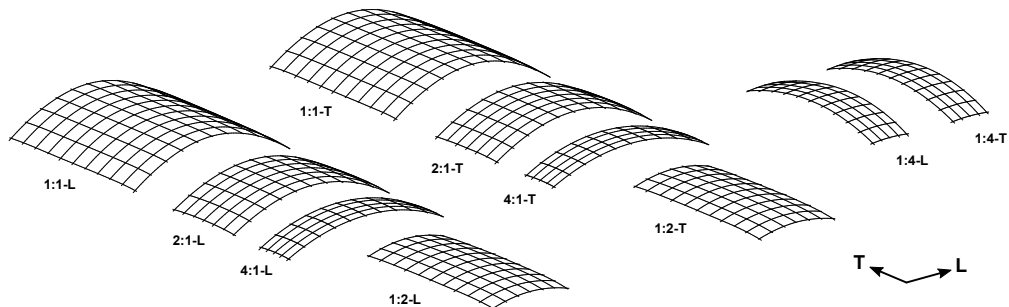
### *3.1. Conventional peen forming experiments*

Figure 6 shows 3D scans of the final deformed shape of sheets used for conventional peen forming experiments and Table 6 lists their curvatures. We see that:

- 205 • Sheets of 1:1 aspect ratio deformed into cylinders;
- Sheets of 1:2 and 2:1 aspect ratio assumed distinct nonzero curvature in both directions, with one of the curvatures being approximately one order of magnitude smaller than the other;
- Sheets of 1:4 and 4:1 assumed elliptical shapes, with curvatures in all  
210 directions having the same order of magnitude;
- All specimens had their largest curvature along the L direction.
- Identical specimens peened with strokes parallel to either the L or the T direction assumed almost identical shapes, with differences in curvatures of less than 7% between the two sets of sheets;

215 These results are consistent with those reported by [8] who observed the same deformed shapes for 4.6 mm thick and 610 mm long 2024-T3 and 7050-T6 aluminum specimens of 4:1, 2:1, 1:1, 1:2, and 1:4 aspect ratio peened with




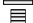





**Figure 6.** 3D scans of 4.9 mm thick and 1016 mm long 2024-T3 aluminum alloy rectangular sheets peened to full coverage at a  $12 \times 10^{-3}$  inches A Almen intensity with SCCW28 shot. All specimens, including 1:4 aspect ratio sheets, had their largest curvature along the L direction. The out of plane displacements were magnified by a factor of 4.

**Table 6**

Average curvatures of peen formed sheets and of the  $254 \times 254$  mm coupons removed from the center of selected sheets.

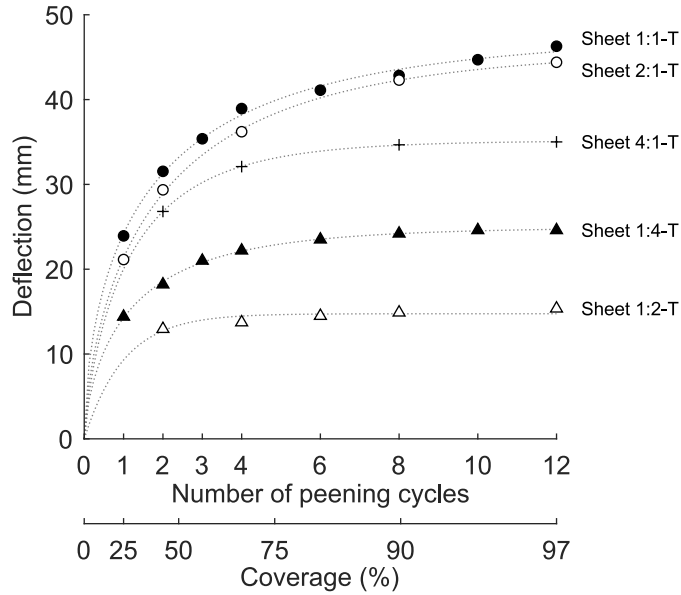
Orientation <sup>†</sup>	Sheets: strokes parallel to L			Sheets: strokes parallel to T			Coupons		
	Specimen	Curvature ( $\times 10^{-4}$ mm <sup>-1</sup> )		Specimen	Curvature ( $\times 10^{-4}$ mm <sup>-1</sup> )		Removed from	Curvature ( $\times 10^{-4}$ mm <sup>-1</sup> )	
		Along L	Along T		Along L	Along T		Along L	Along T
	Sheet 4:1-L	2.50	2.19	Sheet 4:1-T	2.46	2.07	Sheet 4:1-L	2.66	2.14
	Sheet 2:1-L	2.93	0.17	Sheet 2:1-T	3.06	0.11	Sheet 2:1-T	3.12	1.52
	Sheet 1:1-L	3.46	-0.01	Sheet 1:1-T	3.45	$\simeq 0$	Sheet 1:1-L	2.93	1.81
	Sheet 1:2-L	3.56	0.30 <sup>‡</sup>	Sheet 1:2-T	3.52	0.31 <sup>‡</sup>	Sheet 1:2-L	3.03	2.08
	Sheet 1:4-L	3.00	1.81	Sheet 1:4-T	2.93	1.94	Sheet 1:4-L	3.16	1.54

<sup>†</sup> Horizontal lines aligned with the L direction.

<sup>‡</sup> The curvature was approximately constant near the center and transitioned to  $1.2 \times 10^{-4}$  mm<sup>-1</sup> at approximately 200 mm from the edges.

1.7 mm steel shot propelled at 53 m/s (a more intense peening treatment than that used here). Unlike in our experiments, however, Kulkarni's 2024-T3 aluminum specimens had their largest curvature along the T direction.

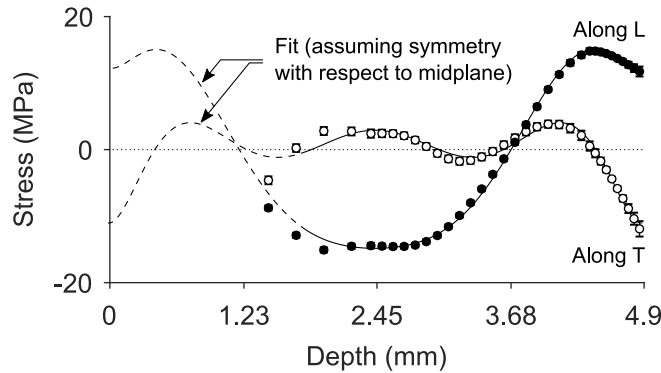
To give a sense of the shape of the sheets at intermediate stages of the peening process, Figure 7 shows the evolution of the deflection as a function of peening time for one sheet of each aspect ratio. These curves show that most of the forming occurred during the first 2 peening cycles, with diminishing returns



**Figure 7.** Deflection of specimens peened with strokes parallel to the T direction versus peening time. Similar curves were obtained for specimens peened with strokes parallel to the L direction. The dotted lines are a least-squares fit of  $f(x) = a(1 - \exp(-bx^c))$ , where  $a$ ,  $b$ , and  $c$  are adjustable parameters.

225 for each additional cycle. After 12 cycles, most sheets had reached saturation, except for 1:1 and 2:1 aspect ratio specimens for which the positive slope suggests that additional peening could have resulted in larger deformations. Similar curves were obtained whether the sheets were peened with strokes parallel to the L or to the T direction.

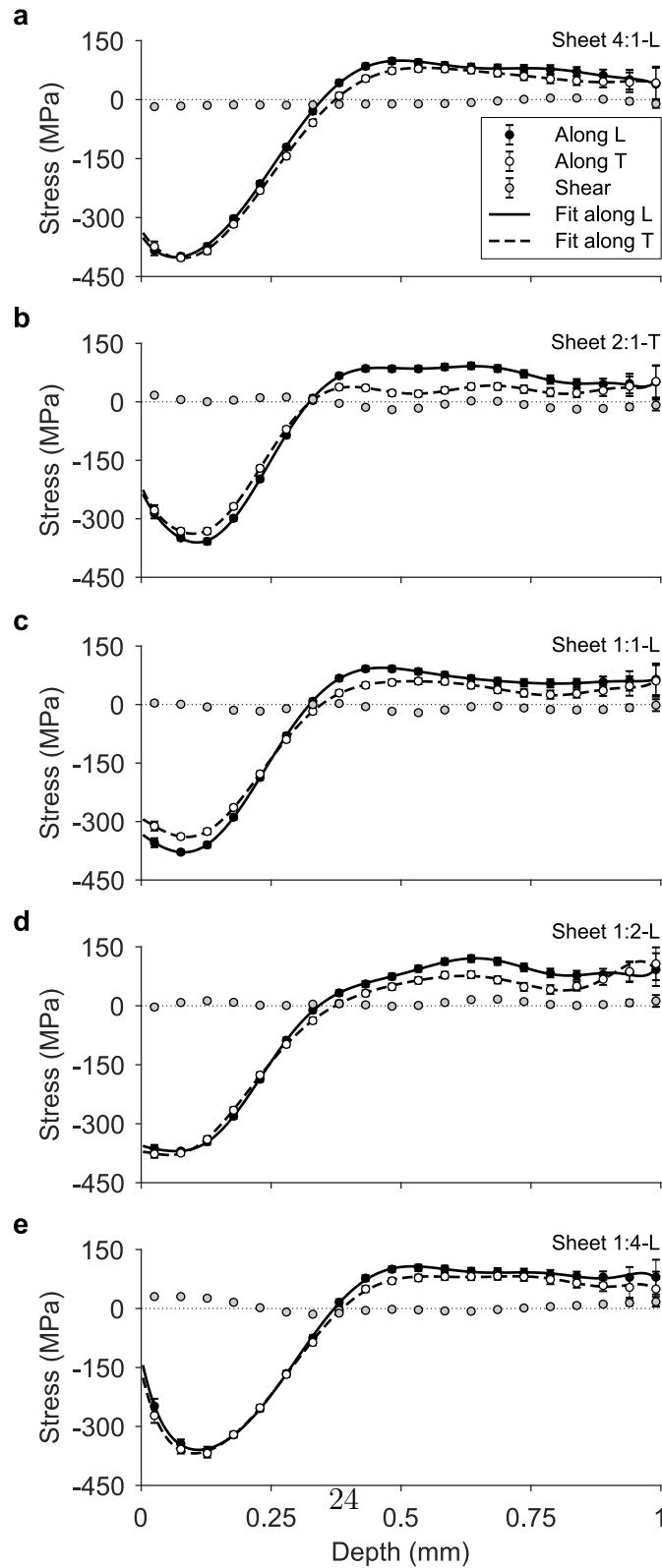
230 Next, we consider the residual stresses inside the sheets. Figure 8 shows initial residual stresses measured by slitting in as-received material. Data were acquired over 70% of the thickness. Because both faces of a sheet experience the same sequence of operations during cold rolling, it is expected that initial residual stresses are symmetric. For this reason, the figure also shows as



**Figure 8.** Residual stresses measured by the slitting method on two  $51 \times 51$  mm coupons removed from an as-rolled sheet. Data were acquired up to a depth of 3.4 mm and through thickness profiles were reconstructed by assuming symmetry with respect to the midplane, fitting a smoothing spline through the cloud of points, and translating the resulting curve along the  $y$  axis to enforce forces equilibrium.

235 dotted lines a reconstruction of the entire residual stress profile obtained by mirroring data points with respect to the midplane of the specimen and by fitting smoothing splines through the cloud of points. The resulting profiles were almost in equilibrium; only a slight translation of 0.15 MPa towards positive stresses was needed to equilibrate axial loads. The shape of the profiles, with tensile stresses in the rolling direction and compressive stresses in the transverse direction, is typical of quenched and stress relieved heat treatable aluminum alloys [37, 38, 39].

245 Figure 9 shows residual stresses measured by hole drilling in  $254 \times 254$  mm coupons removed from the center of the peened sheets. All profiles display maximum compressive residual stresses of approximately  $-380$  MPa. The depth of the plastically deformed layer, that can be inferred from the location of the tensile residual stress peak (see Figure 1c), is about 0.5 mm in all cases.



**Figure 9.** Residual stresses measured by hole drilling at the center of  $254 \times 254$  mm coupons removed from the center of peen formed sheets. The fitting curves—shown only to guide the eye—are polynomial fits.

Note that, because of the stress relaxation that occurred when the coupons were removed from the sheets, residual stresses shown in Figure 9 differ from those that would have been measured in the as-peened sheets.

Finally, Figure 10a shows residual stresses in  $15.24 \times 17.78$  mm coupons evaluated with the slitting method. This measurement was performed to cross-validate hole drilling measurements. In this case, profiles obtained with both methods are close except for the point closest to the surface, which provides the desired validation. Further investigating the differences between both sets of profiles would be hazardous as data were acquired on coupons of different geometries. Besides, hole drilling measurements are local while slitting tends to average stresses along the length of the slot and could be affected by edge effects due to the small size of the coupons.

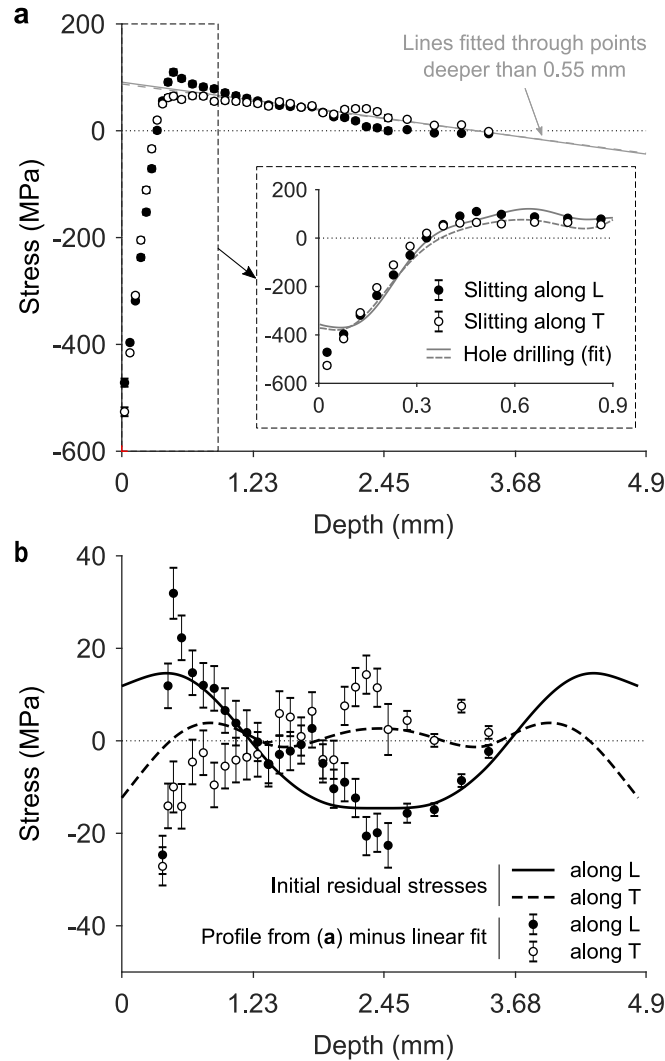
Unlike hole drilling, which can only probe residual stresses in a shallow layer below the peened surface, slitting returns residual stress profiles much deeper into the material. From Figure 10a, it can be seen that, deeper than about 0.6 mm, residual stresses follow a linear trend, with some oscillations that are likely due to initial stresses resulting from the manufacturing process of the sheets. This is confirmed in Figure 10b which shows the same data as in Figure 10a after subtraction of the linear part of the profile alongside the initial stresses from Figure 8. Both sets of profiles have similar shape and magnitude, which is consistent with our understanding of the process: since peening only affects a thin layer of material near the surface, stresses below

270 the plastically deformed layer are equal to the initial stresses plus a linear term due to stretching and bending of the specimens.

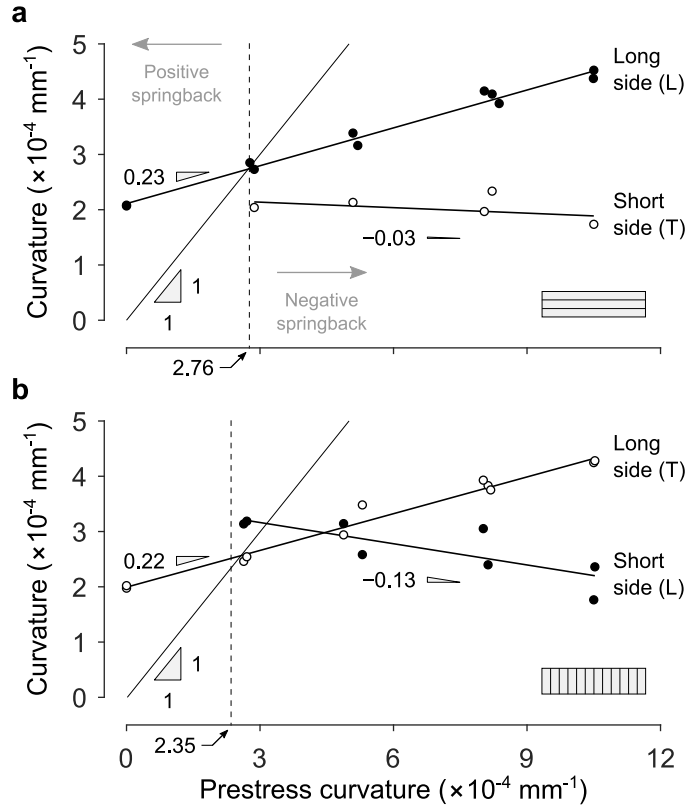
### 3.2. Stress peen forming experiments

Figure 11 shows the final unconstrained curvature of  $508 \times 127$  mm strips used for stress peen forming experiments as a function of prestress curvature. 275 The curvature along the prestress direction increases linearly with a slope of approximately 0.23, regardless of the alignment of the strips with respect to the rolling direction. The curvature along the transverse direction decreases linearly with a slope of  $-0.03$  for strips aligned with the L direction, and with a slope of  $-0.13$  for strips aligned with the T direction. The magnitude of 280 the slopes is consistent with results from the literature compiled in Table 1. To the right of the dashed lines shown in Figure 11, which corresponds to the curvature of identical unconstrained strips peened with the same treatment, the final curvature is smaller than the prestress curvature (negative springback), and vice versa.

285 Figure 12 shows residual stresses measured by hole drilling in  $254 \times 127$  mm coupons removed from the center of strips aligned with the L direction and peened with increasing prestress curvatures. As prestress increases, near surface stresses become more compressive. The largest variations occur along the prestress direction, which causes the profiles to gradually separate. As 290 already noted by [14], prestress appears to have little effect on the depth of the plastically deformed layer. We also observe that, whereas most profiles



**Figure 10.** (a) Residual stresses measured by slitting in  $17.78 \times 15.24$  mm coupons removed from sheet 1:2-L. Superimposed to the data is the fit to the residual stresses measured by hole drilling on the same sheet from Figure 9d. (b) Same data as in (a) after having subtracted the linear portion of the profile caused by bending and stretching of the specimens following peening. The latter was obtained by fitting a line through data points deeper than 0.55 mm. The oscillations thus isolated follow the same trend as that of the initial stresses shown in Figure 8.



**Figure 11.** Average curvatures of  $508 \times 127$  mm strips cut along (a) the L direction and (b) the T direction after all external constraints have been removed. All strips were peened with strokes parallel to their long side. Dashed lines show the curvature that unconstrained identical strips assumed when peened with the same treatment. Above this threshold, the curvatures of the strips are smaller than the prestress curvature (negative springback), and vice versa. Each point corresponds to one specimen. Eleven specimens were damaged before their curvatures along the short side could be measured.



exhibit a local minimum approximately 0.1 mm below the surface, residual stresses in the strip that was held flat during peening do not. Whether this is due to prestress conditions or to variability in hole drilling measurements cannot be assessed from the single profiles reported here.

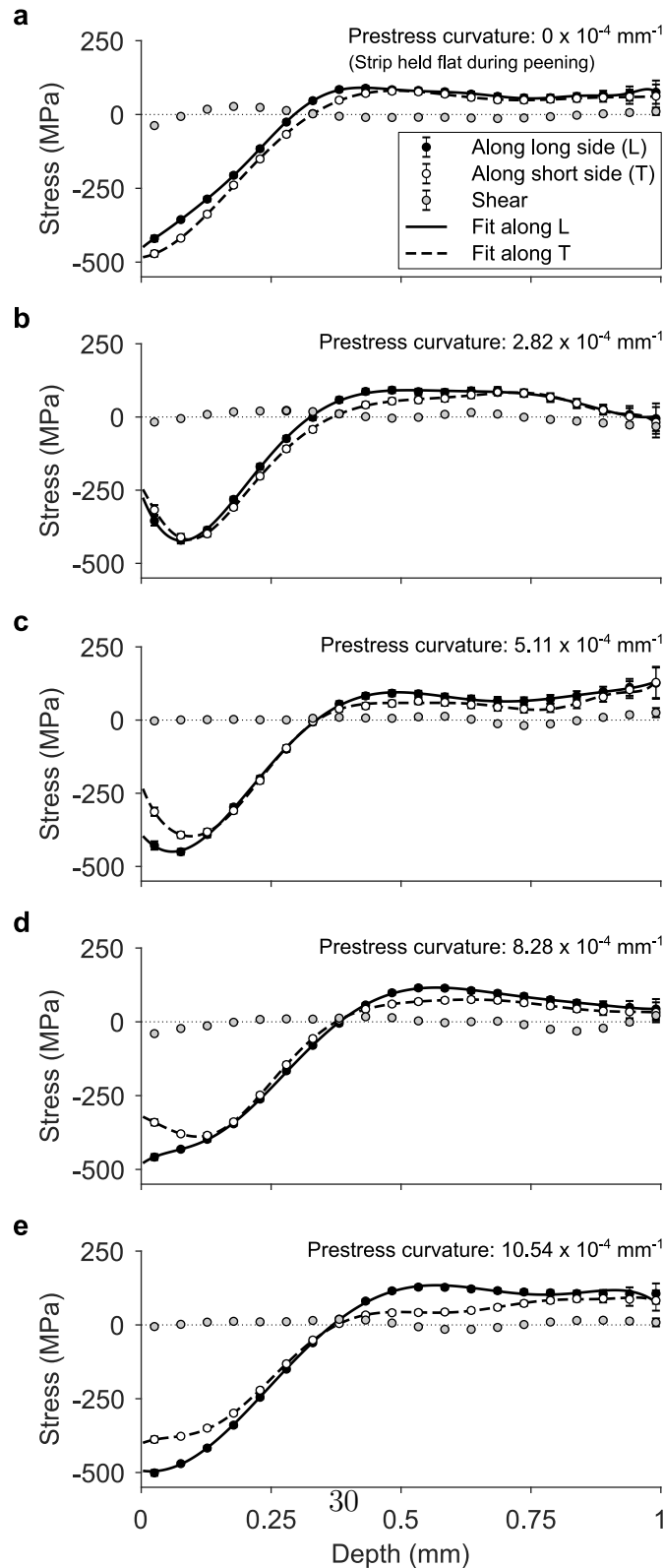
Figure 13 shows residual stresses measured under the same conditions in a coupon removed from a strip that was free to deform during peening. The shape of the profiles is similar to that for other coupons although stresses are approximately 40 MPa higher (i.e., less compressive) over the first 0.2 mm.

Table 7 compares the curvatures of  $508 \times 127$  mm strips that were held flat during peening, prestressed to  $2.7 \times 10^{-4} \text{ mm}^{-1}$ , and unconstrained. Curvatures along the long side of unconstrained strips are reported as dashed lines in Figure 11. Unconstrained strips behave as if they had been prestressed into their final shape, peened, then released: except for curvatures along the short side of strips aligned with the L direction, the curvatures of unconstrained and prestressed strips differs by less than 6%. Their curvature is approximately 25% larger than that of strips that were held flat during peening.

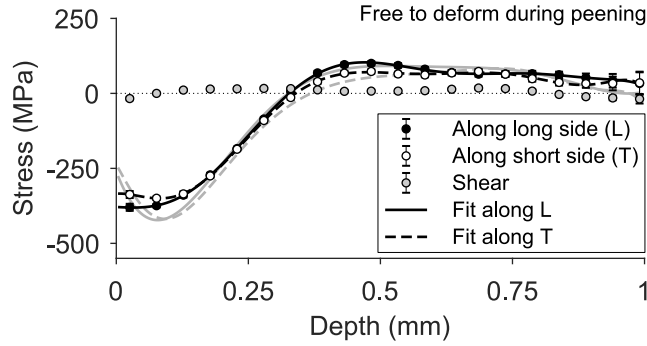
## 4. Discussion

### 4.1. Preliminaries: natural curvatures

To interpret the results of peen forming experiments, a useful tool is the concept of natural curvature. Natural curvature is defined as the curvature



**Figure 12.** Residual stresses measured by hole drilling at the center of  $254 \times 127$  mm coupons removed from the center of strips having their long side aligned with the L direction and peened with increasing prestress curvatures. The fitting curves—shown only to guide the eye—are polynomial fits.



**Figure 13.** Residual stresses measured by hole drilling at the center of a  $254 \times 127$  mm coupon removed from the center of a strip having its long side aligned with the L direction and that was free to deform during peening. The fitting curves—shown only to guide the eye—are polynomial fits. This strip assumed a curvature of  $2.76 \times 10^{-4} \text{ mm}^{-1}$  along the long side. For comparison, the fit to residual stresses measured on the strip prestressed to  $2.82 \times 10^{-4} \text{ mm}^{-1}$  from Figure 12b is shown as light grey curves.

**Table 7**

Curvature of strips that were held flat, prestressed to  $2.7 \times 10^{-4} \text{ mm}^{-1}$  (nominal), and unconstrained during peening. All values  $\times 10^{-4} \text{ mm}^{-1}$ . Reported values were averaged over available results.

Long side aligned with	Held flat		Prestressed to $2.7 \times 10^{-4} \text{ mm}^{-1}$		Unconstrained	
	Along long side	Along short side	Along long side	Along short side	Along long side	Along short side
L	2.08	-	2.79	2.04	2.76	2.75
T	2.00	-	2.50	3.17	2.35	3.16

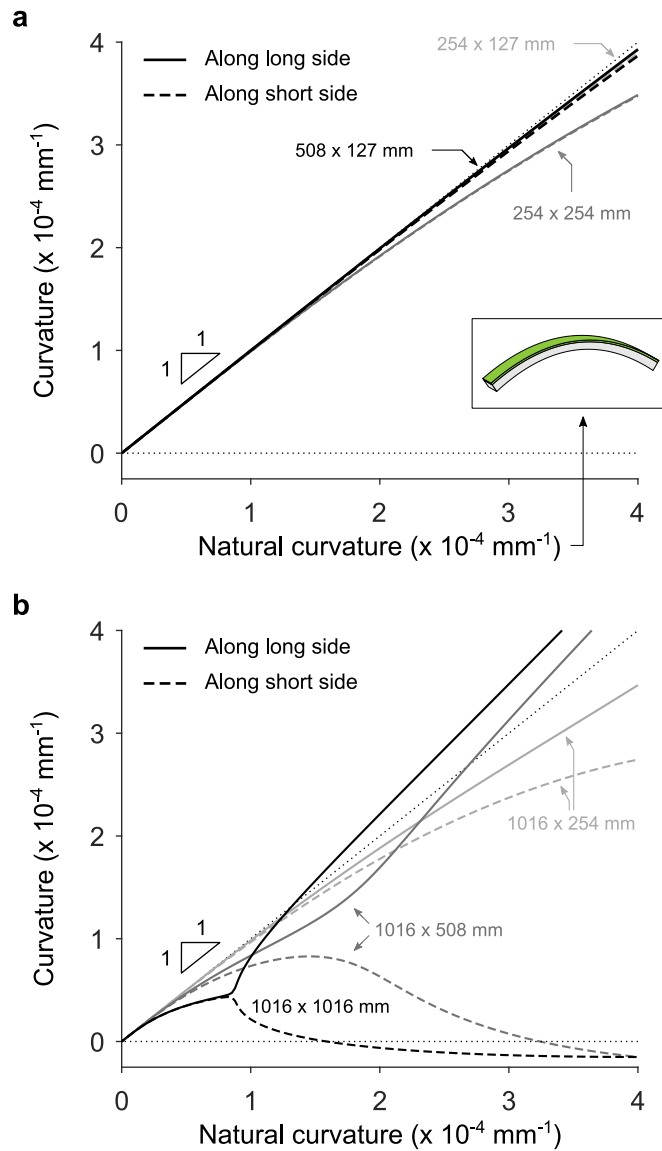
of a small beam cut out from a plate at a given location and along a given direction [40]. It is natural in the sense that it is the curvature that the beam would spontaneously adopt if it were not constrained by surrounding material. The shape of a peen formed plate can therefore be seen as a compromise between the plate reaching its natural curvatures (locally) and satisfying the geometric constraints of plate mechanics (globally). In the case of shot peen parts, natural curvatures only depend on the thickness of the part and in the distribution of peening induced plastic strains.

Now, imagine that a small coupon is carefully removed from a larger shot peened plate and that removal does not alter the distribution of plastic strains in the coupon. If the deflection of the coupon is small compared to its thickness, then its curvatures are close approximations to the natural curvatures. Indeed, the response of a plate when deflections are small is linear and its stretching and bending modes are decoupled. Therefore, the coupon can attain its natural curvature in all directions without the bending in one direction affecting the bending in other directions, see [41, section 23].

This is illustrated in Figure 14a for three geometries: that of strips used for stress peen forming experiments and that of the two types of coupons used for residual stress measurements. These curves were generated using the Abaqus finite element software by prescribing an equibiaxial thermal expansion  $\varepsilon^*$  in the upper half of a plate of thickness  $h$  and by ramping the expansion from zero. The natural curvature of this system is  $3\varepsilon^*/2h$  [42, 43]. The plates

335 were meshed with S4R elements and geometric nonlinearities were included  
in the analysis. For all three geometries, Figure 14a shows that simulated  
curvatures remain close to the natural curvature, even though a small deviation  
is observed for  $254 \times 254$  mm coupons for natural curvatures larger than  
 $2 \times 10^{-4} \text{ mm}^{-1}$ . This deviation is due to nonlinear geometric effects: when  
340 out-of-plane deflections become of the same order as the thickness, stretching  
and bending mode are no longer decoupled and, since the spherical shape  
that the coupons adopt is non-developable, some of the elastic energy must  
contribute to stretching the coupons, which reduces the amount available for  
bending, and results in a stiffening of the structure. Since the curvatures of  
345 prestressed strips (Figure 11) and the curvatures of coupons used for residual  
stress measurements (Table 6) are all smaller than  $4 \times 10^{-4} \text{ mm}^{-1}$ , we  
conclude from Figure 14a that these curvatures are close estimates of natural  
curvatures.

Note that, although the curves in Figure 14a were generated assuming equi-  
350 biaxial expansion, the expansion in the peening affected layer of the actual  
specimens might not be. For example, plastic anisotropy or prestress might  
result in larger expansion in one direction. This, however, does not invalidate  
the fact that curvatures of small rectangular coupons are close approxima-  
tions of natural curvatures when deflections are small.



**Figure 14.** Curvature versus natural curvature for 4.9 mm thick rectangular plates of various dimensions. The curves were obtained from finite element simulations as described in Faucheux et al. [13] assuming equibiaxial expansion in the peening affected layers. (a) For natural curvatures smaller than  $3 \times 10^{-4} \text{ mm}^{-1}$ , the relative difference between the identity line and the curves for  $254 \times 254 \text{ mm}$  plates is less than 8.5%. It is less than 2% for  $508 \times 127 \text{ mm}$  and  $254 \times 127 \text{ mm}$  plates. Therefore, curvatures measured on such specimens are close estimates of natural curvatures. (b) Larger sheets exhibit more complex behaviors. In the linear domain, say for natural curvatures smaller than  $1 \times 10^{-5} \text{ mm}^{-1}$ ,  $1016 \times 1016 \text{ mm}$ ,  $1016 \times 508 \text{ mm}$ , and  $1016 \times 254 \text{ mm}$  sheets deform into spherical shapes. As the natural curvature increases, geometric nonlinear effects become significant and the curves bend downward. When the natural curvature rises above  $1 \times 10^{-4} \text{ mm}^{-1}$ ,  $1016 \times 1016 \text{ mm}$  plates transition to cylindrical shapes due to an elastic instability. For all other geometries, no such transition occurs. Instead, curvatures along the long and short side gradually diverge.

355 *4.2. Explaining the shape of large sheets*

We now turn our attention to the shape of large sheets used for conventional peen forming experiments (Figure 6). Figure 14b shows curvatures as a function of natural curvature for the three geometries considered here. These curves were computed using the same finite element simulations as in  
360 section 4.1. In particular, we still used equibiaxial expansion as loads. Although the expansion in the actual specimens might not be equibiaxial, this simplified model still captures the main features of the response of uniformly peen formed plates.

In the linear domain, say for natural curvatures below  $1 \times 10^{-5} \text{ mm}^{-1}$ , all  
365 specimens deform into spherical shapes and their curvature is the same as the natural curvature. As natural curvature increases, the sheets remain spherical, but the curves depart from linearity due to stress stiffening. Because it is much easier to bend a thin plate than it is to stretch it, cylindrical shapes become energetically favorable for large natural curvatures [40]. For  
370  $1016 \times 1016 \text{ mm}$  plates, the transition occurs suddenly at approximately  $0.86 \times 10^{-4} \text{ mm}^{-1}$ , whereas curvatures along the long and short direction gradually diverge for the two other geometries.

Using the values in Table 6 as estimates for natural curvature, we found that the latter varied between 1.5 and  $3.2 \times 10^{-4} \text{ mm}^{-1}$ , depending on the  
375 specimen and on the direction. In this range, the curves in Figure 14b capture the main features of the experimentally observed deformed shapes: square

plates deform into cylindrical shapes, 2:1 aspect ratio plates into elliptical shapes, and 4:1 aspect ratio plates into nearly cylindrical shapes.

From Figure 14b, we can also infer why specimens peened with strokes parallel to either the L or T direction deformed into identical shapes. For sheets  
380 of 1:1, 1:2, and 2:1 aspect ratio, this was likely because the sheets quickly ‘locked’ into cylindrical shapes, which occurred during the first half of the first peening cycle. Once in this configuration, a sheet can only continue bending in the same direction as its geometric rigidity resists other deformation  
385 modes. The precise peening trajectory is then of little importance if the specimens are peened until their deformation saturates, as was the case here (Figure 7). The same reasoning applies to 1:4 and 4:1 aspect ratio specimens which, although they do not ‘lock’, can only deform into nearly spherical shapes.

#### 390 4.3. Influence of material anisotropy

Simulations in Figure 14 predict that, when the expansion in the peening affected layers is equibiaxial, rectangular sheets spontaneously bend along the long side. This phenomenon was explained by [44] which showed that highly localized regions of double curvature along the free edges of bilayer  
395 systems reduce the elastic energy of the system and make long side bending energetically favorable.

However, not all our specimens bent along the long side. Instead, all had their largest curvature along the L direction, even when the L direction was



aligned with the short side. This is especially clear for 2:1 and 1:2 aspect ratio sheets which—for otherwise identical peening conditions—deformed into cylinders if their long side was aligned with L, and into flatter elliptical shapes if their long side was aligned with T (Figure 6). Because the only difference between these two sets of sheets was their alignment with the rolling direction, these results suggest that some form of material anisotropy resulted in larger expansion in the L direction, with the level of anisotropy being sufficiently strong to overcome the geometrical preference for the sheets to bend along their short side.

Although the 2024–T3 aluminum sheets used here had isotropic elastic properties, tensile tests revealed a mild plastic anisotropy (Table 3). Therefore, we expect that more plastic flow would occur along some direction after each impact, resulting in larger plastic strains, hence curvatures, along this direction. However, it is not clear from the limited tensile test results available that this direction is the L one. Checking that this is the case would require compression or indentation tests.

Another possible source of material anisotropy is the initial residual stresses. Their effect can be explained as follows. In as-received sheets, residual stresses are symmetric with respect to the midplane of the sheets (Figure 8) and, therefore, do not induce curvature. This symmetry, however, is broken when peening induces large compressive residual stresses near the surface. When compared to an initially stress-free specimen, residual stresses on the

back face amplify or reduce the amount of curvature that the specimen experiences, depending on their sign.

#### *4.4. Influence of prestress*

Another source of anisotropy is prestress. Here, we extend the use of the  
425 term ‘prestress’ to designate both externally applied loads (as in stress peen forming experiments) and internal loads (as in conventional peen forming experiments) that cause a sheet to assume a compound curvature. Initial stresses before an impact depend on the direction of the prestress and cause larger plastic strains to develop in the direction in which stresses are the  
430 largest (i.e., the more tensile, or the less compressive).

This effect is most clearly seen in the curvature of strips used for stress peen forming tests which is always larger along the prestress direction (Figure 11). It also affects the shape of unconstrained sheets that were free to deform during peening as evidenced by the fact that coupons removed from specimens  
435 used for conventional peen forming tests all had different curvatures. Indeed, recall that the curvatures of the coupons are close estimates of natural curvature, and that the latter only depends on the thickness of the coupon and on the distribution of plastic strains. Had the progressive deformation of the specimen hadve no effect, all coupons would have assumed the same curva-  
440 tures since they were removed from specimens made from the same material and peened in the same conditions.

This effect is also apparent in Figure 7 which shows that the deflection of

445 sheets of different geometries saturated after different numbers of peening cycles. For example, sheet 1:2-T saturated after approximately five cycles whereas sheets 1:1-T and 2:1-T had not reached saturation after twelve cycles. Had the progressive deformation of the specimen had no effect, all curves would have saturated at the same time.

450 Finally, notice how residual stresses measured in coupons removed from sheets 2:1-T and 1:1-L, which deformed into cylindrical shapes, exhibited larger compressive stresses along the bending direction (Figure 9b-c) whereas residual stresses in coupons removed from other sheets, which deformed into elliptical or nearly spherical shapes, were almost equibiaxial (Figure 9a, d, e).

## 5. Conclusion

455 In this paper, we presented the results of conventional and stress peen forming experiments conducted on 4.9 mm thick 2024-T3 aluminum sheets shot peened to full coverage with the same low intensity treatment. Our results highlight features of the response of thin peen formed sheets that were known to process engineers but that had been poorly documented so far. In particular, we illustrated why squares are susceptible to elastic instabilities but elongated strips less so, and we showed that the final shape of a peen formed sheet does depend on the way the sheet deforms during peening—this deformation having the same effect as an externally applied prestress. We also observed

a preferential bending of all specimens along the L directions and discussed  
465 why this behavior must be a manifestation of material anisotropy—in the  
form of plastic anisotropy or non-equibiaxial initial stresses inherited from  
earlier processing stages (e.g., heat treatment, rolling).

The other main observations are as follows.

1. Identical specimens peened until their deformation saturated assumed  
470 identical shapes, regardless of the peening trajectory.
2. The curvatures of prestressed strips varied linearly with the prestress  
curvature.
3. There exists a critical prestress curvature such that, when constraints  
are removed, a prestressed strip does not spring back. This curvature  
475 coincides with that which the strip would assume if it was free to deform  
during peening.
4. If a strip is prestressed to a smaller curvature than this critical value  
(for example, if it is held flat during peening), it will bend less than if  
it is free to deform, and vice versa.

480 Although similar behaviors were observed in earlier works, residual stress  
measurements along both directions before and after peening were seldom  
reported. This information is needed to understand how different sources of  
anisotropy—such as prestress, plastic anisotropy, and non-equibiaxial initial  
stresses—affect the final deformed shapes. Furthermore, such measurements  
485 enable to identify peening-induced plastic strains which provide much clearer

insights into the mechanics of peen formed plates than residual stresses alone.

## 6. Acknowledgements

The authors gratefully acknowledge financial support from Airbus, from the Rio Tinto group through a graduate scholarship, from the Canada Research  
490 Chairs program, and from the Natural Sciences and Engineering Research Council of Canada (NSERC; funding reference number 175791953). The prestressing jig used for stress peen forming experiments was courtesy of Aérospère and Centre Technologique en Aérospatiale (CTA).

## References

- 495 [1] D. L. Baughman, Peen forming, *Machine design* 42 (1970) 156–160.
- [2] A. Levers, Broughton: From Wellington bombers to the A380, *The International Journal for the History of Engineering & Technology* 80 (2010) 55–79.
- [3] K. Hornauer, W. Köhler, Development of the peen forming process for  
500 spherical shaped components, in: *Proceedings of the 4th International Conference on Shot Peening (ICSP4)*, Tokyo, Japan, 1990, pp. 585–594.
- [4] J. Merino, A. Patzelt, A. Steinacher, M. Windisch, G. Heinrich, R. Forster, C. Bauer, *Ariane 6 - Tanks & structures for the new european launcher*, München, 2017, p. 10.

- 505 [5] R. D. Skinner, Stress-peen straightening of complex machined aircraft parts, in: *Formability Topics—Metallic Materials*, ASTM International, 1978, pp. 100–121.
- [6] J. Eckersley, D. Axline, B-727 brake components salvaged by shot peen forming, in: *Proceedings of the 27th annual aerospace/airline plating and metal finishing forum*, San Antonio, Texas, US, 1991.
- 510 [7] A. Gariépy, Finite element modelling of shot peening and peen forming processes and characterisation of peened AA2024-T351 aluminium alloy, Ph.D. thesis, École Polytechnique de Montréal, 2012.
- [8] K. M. Kulkarni, J. A. Schey, D. V. Badger, Investigation of shot peening as a forming process for aircraft wing skins, *Journal of Applied Metalworking* 1 (1981) 34–44.
- 515 [9] A. P. Villalva-Braga, Análise de ligas de alumínio aeronáuticas conformadas por jateamento com granalhas-caracterização e previsão de deformação, Master’s thesis, Universidade de São Paulo, 2011.
- 520 [10] H. Y. Miao, D. Demers, S. Larose, C. Perron, M. Lévesque, Experimental study of shot peening and stress peen forming, *Journal of Materials Processing Technology* 210 (2010) 2089–2102.
- [11] M. B. Prime, Amplified effect of mild plastic anisotropy on residual stress and strain anisotropy, *International Journal of Solids and Structures* 118-119 (2017) 70–77.
- 525

- [12] A. Gariépy, S. Larose, C. Perron, P. Bocher, M. Lévesque, On the effect of the orientation of sheet rolling direction in shot peen forming, *Journal of Materials Processing Technology* 213 (2013) 926–938.
- [13] P. A. Fauchaux, F. P. Gosselin, M. Lévesque, Simulating shot peen forming with eigenstrains, *Journal of Materials Processing Technology* 254 (2018) 135–144.
- [14] C. F. Barrett, R. Todd, Investigation of the effects of elastic pre-stressing technique on magnitude of compressive residual stress induced by shot peen forming in thick aluminum plates, in: *Proceedings of the Second International Conference on Shot Peening*, Chicago, 1984, pp. 15–21.
- [15] Y. Hu, Z. Li, X. Yu, Z. Yao, Effect of elastic prestress on the laser peen forming of aluminum alloy 2024-T351: Experiments and eigenstrain-based modeling, *Journal of Materials Processing Technology* 221 (2015) 214–224.
- [16] K. Li, Using stress peen-forming process for integrally stiffened wing panels, in: *Proceedings of the First International Conference on Shot Peening*, Paris, France, 1981, pp. 555–563.
- [17] H. Miao, S. Larose, C. Perron, M. Lévesque, Numerical simulation of the stress peen forming process and experimental validation, *Advances in Engineering Software* 42 (2011) 963–975.

- [18] M. T. Wang, Y. S. Zeng, X. P. Bai, X. Huang, Deformation rule of 7150 aluminum alloy thick plate by pre-stress shot peen forming, *Advanced Materials Research* 1052 (2014) 477–481.
- [19] X. Xiao, Y. Wang, W. Zhang, J. Wang, S. Wei, Numerical research on stress peen forming with prestressed regular model, *Journal of Materials Processing Technology* 229 (2016) 501–513.
- [20] T. Zhang, L. Li, S.-h. Lu, J.-b. Zhang, Z. Zhou, H. Gong, Effect of prestressed ultrasonic peen forming parameters on bending curvature and spherical deformation of plate, *Transactions of Nonferrous Metals Society of China* 29 (2019) 270–278.
- [21] SAE standard J2277, Shot Peening Coverage Determination, Standard, SAE International, 2013.
- [22] SAE standard J443, Procedures for Using Standard Shot Peening Almen Strip, Standard, SAE International, 2010.
- [23] W. Cao, R. Fathallah, L. Castex, Correlation of Almen arc height with residual stresses in shot peening process, *Materials science and Technology* 11 (1995) 967–973.
- [24] B. Cina, T. Kaatz, I. Eldror, The effect of heating shot peened sheets and thin plates of aluminium alloys, *Journal of materials science* 25 (1990) 4101–4105.



- [25] M. Gelineau, Étude de l'impact du grenailage sur des composants mécaniques industriels à géométrie complexe, Ph.D. thesis, École Nationale Supérieure d'Arts et Métiers, 2018.
- [26] W. Johnson, A. G. Mamalis, S. K. Ghosh, On the peen-forming of metals, in: Proceedings of the Twenty-First International Machine Tool Design and Research Conference, Palgrave, London, 1981, pp. 85–93.
- [27] A. Gariépy, S. Larose, C. Perron, M. Lévesque, Shot peening and peen forming finite element modelling – Towards a quantitative method, International Journal of Solids and Structures 48 (2011) 2859–2877.
- [28] ASTM standard B557M-15, Standard test methods for tension testing wrought and cast aluminum- and magnesium-alloy products (metric), Standard, ASTM International, West Conshohocken, PA, 2015.
- [29] F. Bron, J. Besson, A yield function for anisotropic materials. Application to aluminum alloys, International Journal of Plasticity 20 (2004) 937–963.
- [30] J. Seidt, A. Gilat, Plastic deformation of 2024-T351 aluminum plate over a wide range of loading conditions, International Journal of Solids and Structures 50 (2013) 1781–1790.
- [31] AMS standard 2431/8B, Peening Media (AWCH) Conditioned Carbon Steel Cut Wire Shot, High Hardness (55 to 62 HRC), Standard, SAE International, 2007.

- [32] AMS standard 2430 rev. T, Shot Peening, Automatic, Standard, SAE International, 2015.
- [33] M. B. Prime, Residual stress measurement by successive extension of a slot: The crack compliance method, *Applied Mechanics Reviews* 52 (1999) 75–96.
- [34] G. S. Schajer, M. B. Prime, Use of inverse solutions for residual stress measurements, *Journal of Engineering Materials and Technology* 128 (2006) 375.
- [35] M. B. Prime, M. R. Hill, Uncertainty, model error, and order selection for series-expanded, residual-stress inverse solutions, *Journal of Engineering Materials and Technology* 128 (2006) 175–185.
- [36] ASTM standard E837-08, Standard Test Method for Determining Residual Stresses by the Hole-Drilling Strain-Gage Method, Standard, ASTM International, West Conshohocken, PA, 2008.
- [37] G. E. Dieter, Mechanical metallurgy, Metallurgy and Metallurgical Engineering Series, McGraw-Hill, New York, 1961.
- [38] M. B. Prime, M. R. Hill, Residual stress, stress relief, and inhomogeneity in aluminum plate, *Scripta Materialia* 46 (2002) 77–82.
- [39] J. S. Robinson, D. A. Tanner, C. E. Truman, The origin and management of residual stress in heat-treatable aluminium alloys: Origin and management of residual stresses, *Strain* 50 (2014) 185–207.

- [40] M. Pezzulla, G. P. Smith, P. Nardinocchi, D. P. Holmes, Geometry and mechanics of thin growing bilayers, *Soft Matter* 12 (2016) 4435–4442.
- 610 [41] S. Timoshenko, *Strength of materials; Part II; Advanced theory and problems*, 2nd ed. ed., D. Van Nostrand Company, Inc., 1940.
- [42] S. Timoshenko, Analysis of bi-metal thermostats, *Journal of the Optical Society of America* 11 (1925) 233–255.
- [43] W. M. van Rees, E. Vouga, L. Mahadevan, Growth patterns for shape-  
615 shifting elastic bilayers, *Proceedings of the National Academy of Sciences* 114 (2017) 11597–11602.
- [44] S. Alben, B. Balakrisnan, E. Smela, Edge effects determine the direction of bilayer bending, *Nano Letters* 11 (2011) 2280–2285.